3.1 INTRODUCTION

This chapter deals with the removal of fluoride by adsorption from the aqueous solution using rGO/ZrO_2 nanocomposite. Fluoride plays an essential role in the process of bone formation, and it also helps to prevent the tooth decay when its concentration present within the recommended limit (WHO recommend the 1.5 mg/L). Whereas, the excess concentration of fluoride causes various harmful consequences in the human body such as dental fluorosis, skeletal fluorosis, brittle bones, osteoporosis, arthritis, cancer, immunological and congenital disabilities [Wang *et al*. (2007), Harrison (2005), Valdez-Jiménez *et al*. (2011)]. The high amount of the fluoride contaminates the water by various natural as well as by the anthropogenic activity. Water get contaminated by dissolution and weathering of fluoride-bearing minerals i.e. apatite, fluorite, rock phosphate and topaz [Teotia *et al.* (1981)]. Different industrial discharge also polluted the water with the elevated concentration of fluoride such that electroplating, coal, semiconductor manufacturing, aluminum smelter, ceramic production where fluoride used as a necessary ingredient [Kumar *et al.* (2009)]. Water pollution by fluoride become the major global concern. Various technologies have been reported to remove fluoride from water among them adsorption method found to be more effective and economical [Sarkar *et al.* (2006)]. In this investigation, the nanocomposite of the rGO/ZrO_2 has been used for the removal of fluoride from water by batch adsorption experimentation.

Zirconium ions and Zirconium containing materials supposed to show high affinity toward fluoride. Zr (IV) show similar characteristic as alumina and show specific binding affinity for fluoride i.e. F^- is a hard base whereas, Zr^{4+} is a hard acid, and thus these ions reported to exhibit strong hard acid-base interaction [Rafique *et al.*(2012), Wang *et al.* (2009), Liu and Lin (2005)]. In addition, the Zr (IV) ion shows

chemical inertness, high thermal stability, insolubility in water and amphoteric behavior which makes it environment-friendly and excellent adsorbent for fluoride [Luo *et al.* (2013)]. Besides all these properties, it also exhibits the insolubility over wide pH range, biocompatible, economical to produce, thermally stable and highly electrochemically active [Pan *et al.* (2013)]. Zr(IV) ions in the hydrated state usually form tetrameric or octameric species which are bonded with a large number of hydroxyl ions and water molecules hence; actively participate in ligand exchange reaction with fluoride [Zhang *et al.* (2012)]. This fact is well supported by the literature that the Zr(IV) impregnated carbon material showed 3-5 times enhance adsorption performance [Velazquez-Jimenez *et al*. (2013)]. In the present era from the family of carbon nanomaterial, the graphene oxide become important member and proved to be excellent adsorptive material due to its high surface area and existence of abundant oxygen functional groups such that hydroxyl, epoxy groups and carboxylic [Dreyer *et al.* (2010), Barathi *et al.* (2014)]. Literature study also revealed that the graphene and its composites are reported to be effective adsorbent and sensor specifically for the fluoride [Li *et al*. (2011), Poursaberi *et al.* (2012), Li *et al*. (2013a)]. Thus, the modification of graphene oxide with suitable metal ions may result in the formation of a promising adsorbent for fluoride. It is well reported by many researchers that composites of graphene oxide and metal oxide show good adsorption capacity for fluoride in which graphene oxide act as a host which hold the nanoparticles on its surface and keep them in disperse form [Li et al. (2013b), Chen *et al*. (2013)]. However, nanoparticles upon attachment become the barrier in between graphene layers and resist them to restack consequently, provides structural rigidity. Therefore, the nanocomposite of graphene oxide and zirconium oxide expected to show elevated uptake capacity for fluoride. In

this study, the nanocomposite of graphene oxide and zirconium oxide (rGO/ZrO_2) has prepared by hydrothermal method. Moreover, the reduced graphene oxide which formed during the procedure also takes part in adsorption process as its surface become less negative due to reduction thus does not repel the negatively charges fluoride. The detailed kinetic, isotherm and thermodynamic studies were also carried out for the adsorption of fluoride.

3.2 MATERIAL AND METHOD

3.2.1 Synthesis of rGO/ZrO_2 nanocomposite

The starting material GO was prepared by modified Hummer's method, and its detailed procedure is given in chapter 2 (section 2.3). The rGO/ZrO_2 nanocomposite was prepared by a simple one-step hydrothermal method in which $ZrOCl_2.8H_2O$ act as the ZrO_2 precursor and GO plays the role of supporting material. In this procedure, 0.07 g of GO was dispersed uniformly into the 50 mL DW by ultrasonication for two h. In another beaker 30 mL, an aqueous solution of $ZrOCl_2.8H_2O$ (0.03M) was taken and stirred vigorously for 30 min. After that, the GO suspension was added to the solution of $ZrOCl_2.8H_2O$ with stirring. Then the final mixture was ultrasonicated for 1 h followed by addition of 1 ml of hydrazine hydrate to it, and the mixture was placed in a stainless steel teflon lined autoclave at 180°C for 18 h. The black colored composite thus obtained was separated by centrifugation and then repeatedly washed with distilled water and subsequently by ethanol. In the last step, the collected rGO/ZrO_2 nanocomposite was dried for overnight at 120°C. Then the rGO and ZrO_2 nanoparticles were also prepared by the same method but without the addition of $ZrOCl_2.8H_2O$ and GO respectively.

3.2.2 Experimental methodology

The synthesis of rGO/ZrO_2 nanocomposite and its physical as well as chemical properties were characterized with different characterization tools such as FT-IR, XPS, SEM, EDx, Raman spectroscopy, XRD, BET and pHzpc measurement. The prepared nanocomposite was utilized for fluoride removal of fluoride by batch method. The effect of different process parameters were studied by altering the solution pH (2-11), contact time (5-80 min), rGO/ZrO_2 dose (0.4-0.6 g/L), initial fluoride concentration (5-50 mg/L) and temperature (20-40°C). The detailed kinetic, isotherm and thermodynamic studies were also conducted.

3.3 CHARACTERIZATION OF rGO/ZrO_2 NANOCOMPOSITE

3.3.1 FTIR Analysis

FTIR analysis provides elementary information about different functional groups present in the adsorbent. Figure 3.1 represents the FTIR spectra of GO, ZrO_2, and rGO/ZrO_2. A broad and intense peak at 3266 cm^{-1} ascribed for the O-H stretching vibration corresponding to the physisorbed water molecules which is observed in all the three spectra. GO showed its featured peaks at 1724 cm^{-1} (C=O stretching vibration of -COOH), 1618 cm^{-1} (O-H bending vibration of water molecules and C-C skeleton vibration of GO), 1396 cm^{-1} (O–H bending vibration of C-OH and -COOH), 1245 cm^{-1} (C–O stretching vibration of epoxy and ethers) and 1062 cm^{-1} (C-O-C stretching vibration). The spectrum corresponding to the ZrO_2 shows the peak at 619 cm^{-1} [Shan and Gao (2005)] which is attributed to the stretching vibration Zr-O bond. Whereas, the FTIR spectrum of the nanocomposite (rGO/ZrO_2) showed the shift in characteristic vibration peak of C=O from 1724 to 1741 cm^{-1} and the intensity of the peak also decreased due to interaction with Zr(IV) [Zhou *et al*. (2015)].

Besides the peak below 700 cm^{-1} assigned to the characteristic peak of ZrO_2 [Shan and Gao (2005)]. Thus, it was concluded that ZrO_2 is successfully attached on the GO surface.

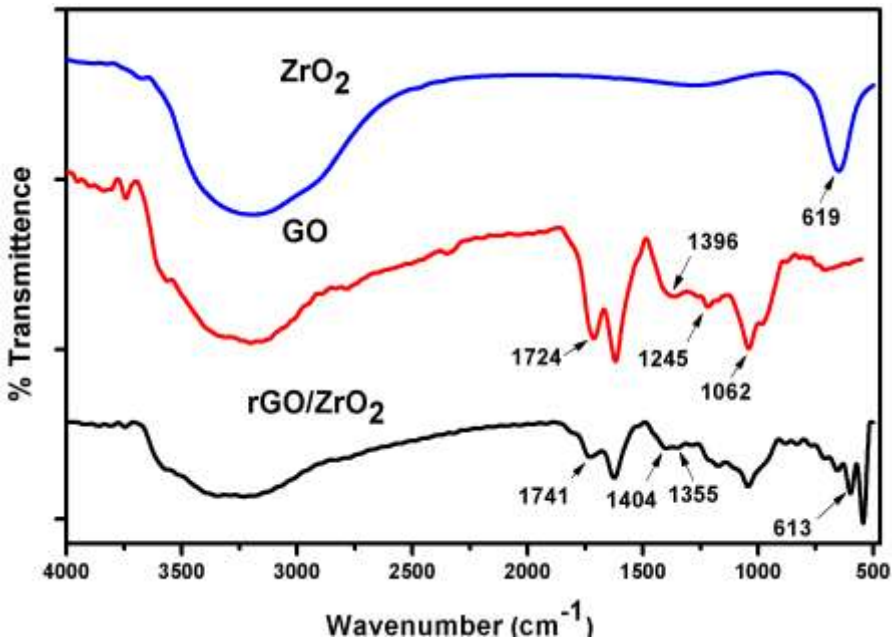

Figure 3.1. FT-IR spectra of GO, rGO/ZrO_2, and ZrO_2

3.3.2 XRD Analysis

The crystalline structure of prepared adsorbent was examined by XRD analysis, and Figure 3.2 shows the XRD pattern of the GO, rGO, ZrO_2, and rGO/ZrO_2. XRD pattern of GO shows the distinct peak at 2θ = 10.8° attributed to the 002 reflection plane and d spacing observed to be 0.85nm. The interlayer spacing (d-spacing) in between the individual layers of the pristine graphite was observed to be 0.34 nm which is less in comparison of the graphene oxide which confirmed the oxidation of graphene

oxide from graphite [Mishra *et al.* (2014)]. The XRD pattern of rGO showed its characteristic broad peak at 2 θ = 24.2°. The XRD pattern of ZrO_2 showed the featured peak at 2θ= 29.9°, 34.7°, 43.02°, 52.2° which corresponds to the tetragonal structure of the ZrO_2 nanoparticles and the peaks were well matched with the JCPDS card, file No.89-7710. The reduction of GO to rGO was confirmed by the XRD pattern of the rGO/ZrO_2 nanocomposite in which characteristic peak of GO was not observed at the low 2θ value [Teymourian *et al.* (2014)]. XRD analysis of prepared nanocomposite shows the peak of rGO as well as ZrO_2 which again supported the successful formation of the rGO/ZrO_2 nanocomposite.

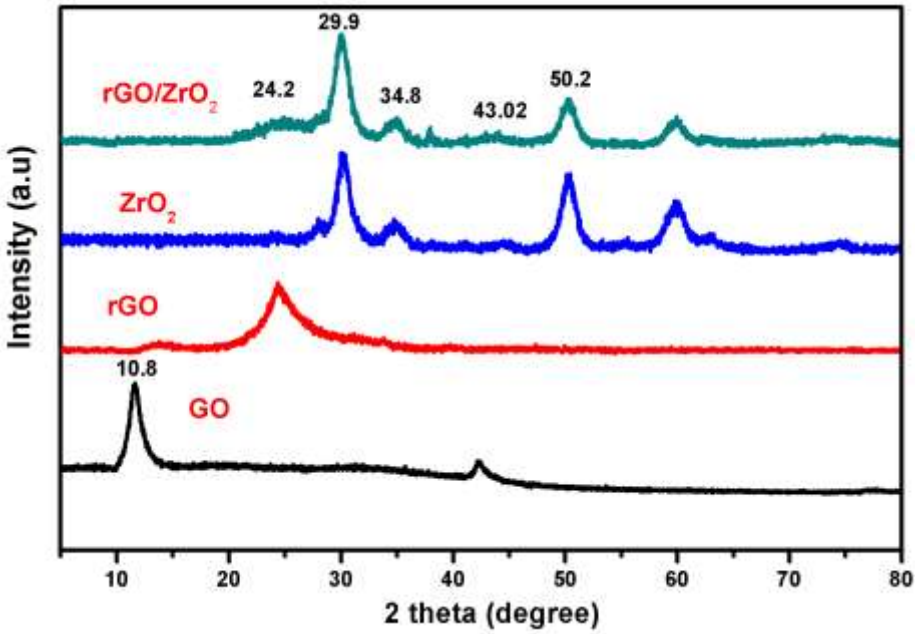

Figure 3.2 XRD pattern of GO rGO, ZrO_2 and rGO/ZrO_2

3.3.3 XPS Analysis

XPS analysis of the adsorbent was performed before and after the adsorption. The wide scan spectra of the rGO/ZrO_2 shows the photoelectron lines characteristics of the C1s, O1s, and Zr3d which revealed the presence of carbon, oxygen and zirconium element in the composite (Figure 3.3 a and b).

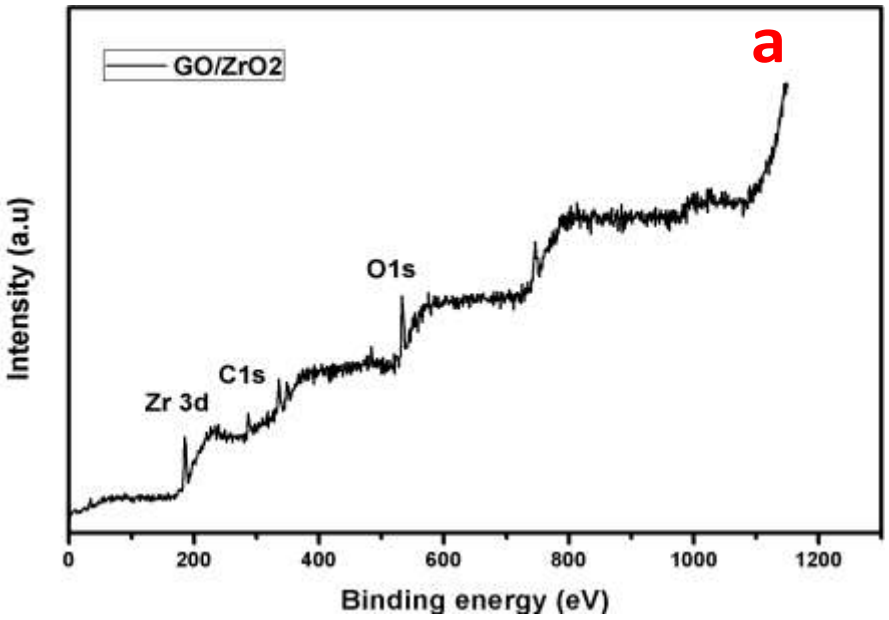

Figure 3.3a Wide scan XPS spectra of rGO/ZrO_2

The core level C1s XPS spectrum of GO shown in Figure 3.3c and the signals was observed at 284.7 eV (C-C/C=C), 286.7 eV (C–OH), 288.1 eV (C=O), and 289.1 eV (C=O–OH) indicated the presence of four different oxygen functionalities of the graphene oxide. Whereas, the Figure 3.3d shows the core level spectra of C1s after nanocomposite formation in which all the four carbon functional group present but of reduced intensity which advocated that GO was reduced during the nanocomposite

formation. Besides as additional peak was also observed at 285.6 eV attributed to the C of the C-N bond of hydrazine which was used in the synthesis procedure and involved in the reduction of graphene sheets [Zhou *et al.* (2015)]. The core level spectra of Zr represented in Figure 3.3e in which the peaks observed at 183.5 and 185.7 eV which was attributed to the spin–orbit splitting of $Zr3d_{5/2}$ and $Zr3d_{3/2}$ component of the Zr3d [Vilian *et al*. (2014)]. XPS analysis in this work also helps us to study the mechanism of fluoride adsorption. Thus the XPS analysis of the nanocomposite before and after the adsorption was performed and it was observed that the additional peak of F1s at 684.75 eV was found in the wide scan spectrum of the nanocomposite after the adsorption (Figure 3.3 b). Furthermore, the XPS spectrum of Zr3d before and after adsorption (Figure 3.3e) was also recorded, and it was revealed that the Zr3d peaks shifted from 184.4 eV to 184.8 eV which confirm the interaction of fluoride with the Zr(IV) [Qiusheng *et al*. (2015)].

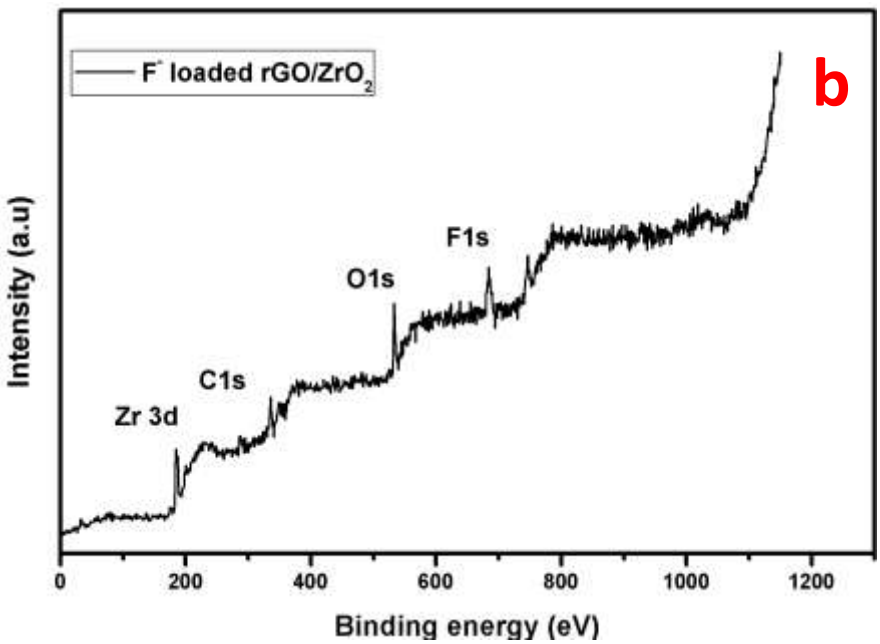

Figure 3.3b Wide scan XPS spectra of rGO/ZrO_2 after fluoride adsorption

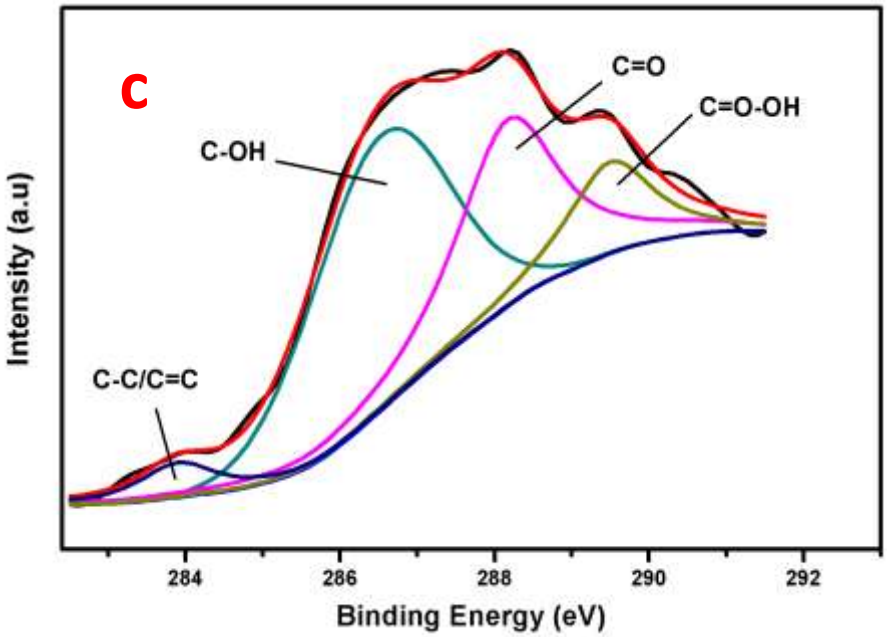

Figure 3.3c Core level C1s spectrum of GO

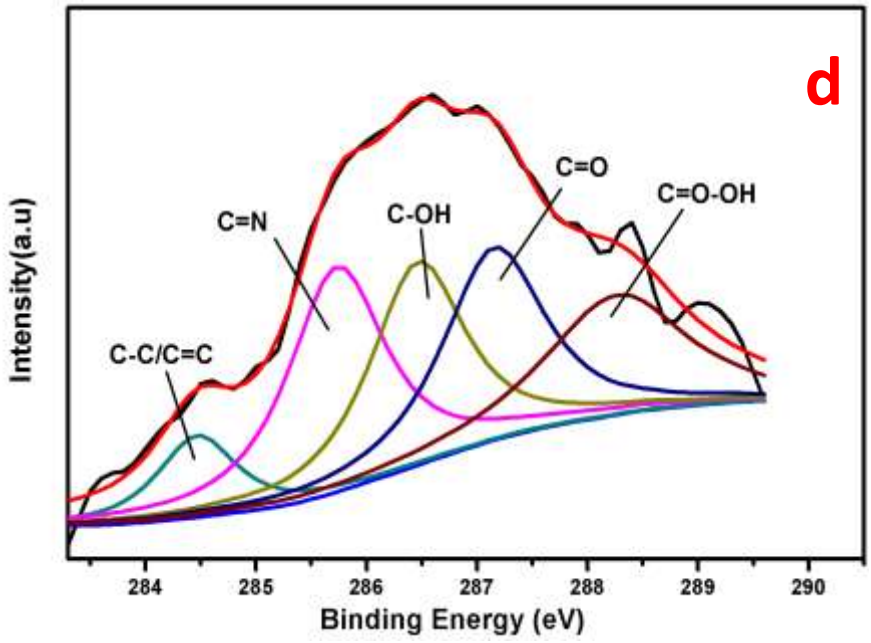

Figure 3.3d Core level C1s spectrum of rGO/ZrO_2

Additionally, the peak of $Zr3d_{3/2}$ and $Zr3d_{5/2}$ shifted toward higher binding energy and also broadened due to the interaction of fluoride with the zirconium which may be due to the formation of the new Zr-oxyfluoride complex. The shifting in the Zr peaks observed due to the fact that when Zr got attached with the fluoride which is more electronegative that Zr then the electron density shifted toward the fluoride which is the cause of peak shifting [Dou *et al.* (2012].

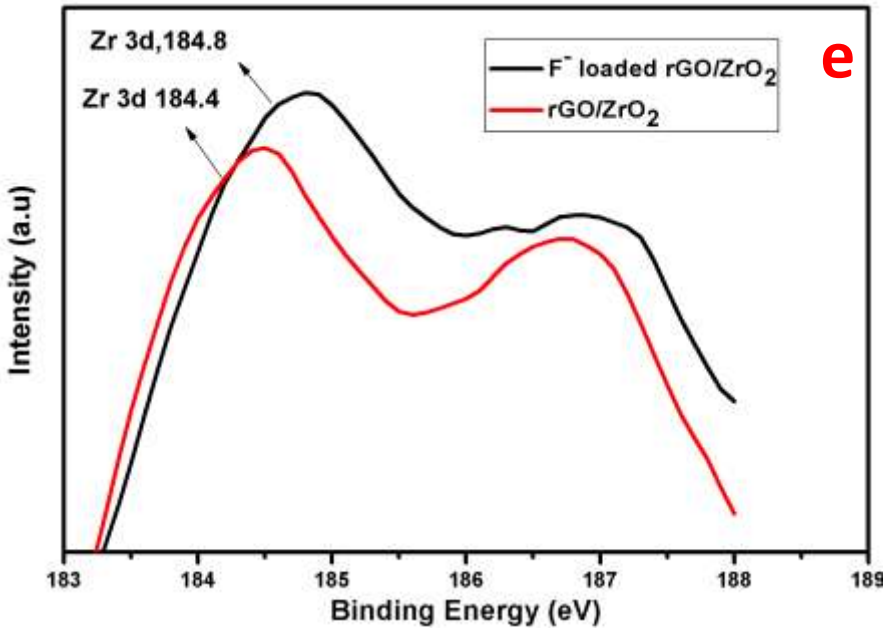

Figure 3.3e Core level Zr3d spectrum of rGO/ZrO_2

3.3.4 SEM and EDX analysis

Figure 3.4a represent the typical morphology of the graphene i.e. wrinkled and stacked graphene layers. Whereas, the SEM micrograph of the rGO/ZrO_2 showed the graphene sheets on which abundant ZrO_2 nanoparticles are evenly distributed (Figure 3.4b). Figure 3.4c displayed the SEM micrograph of rGO/ZrO_2 nanocomposite at high magnification in which a large number of ZrO_2 nanoparticles having the average size of 35 nm are attached on the surface of rGO is clearly seen. The EDX spectrum of GO

(Figure 3.5a) showed the signal for C and O while the spectrum of rGO/ZrO2 nanocomposite (Figure 3.5b) showed signal corresponding to the C, O, and Zr. The signal of Zr reveals the successful incorporation of ZrO_2 on the GO surface. The adsorption of fluoride on the rGO/ZrO_2 surface was confirmed by the EDX spectrum of rGO/ZrO_2 after the adsorption which contains the signal for fluoride in addition to C, O, and Zr (Figure 3.5c). The elemental mapping analysis was also performed on the rGO/ZrO_2 which is shown in Figure 3.6 which was also advocated for homogenous distribution of ZrO_2 nanoparticles on the rGO surface.

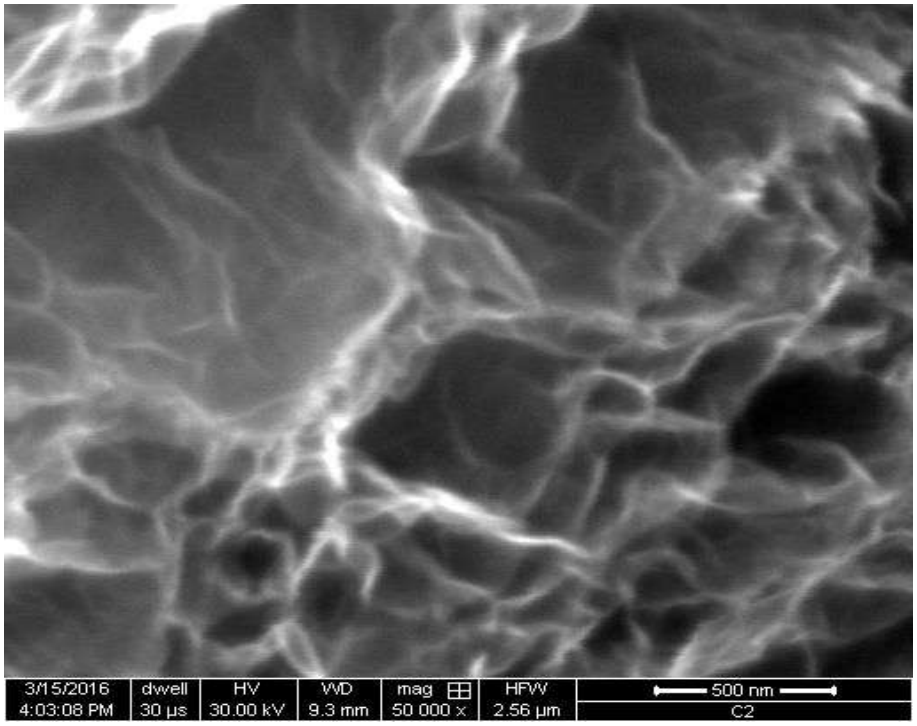

Figure 3.4 (a) SEM image GO

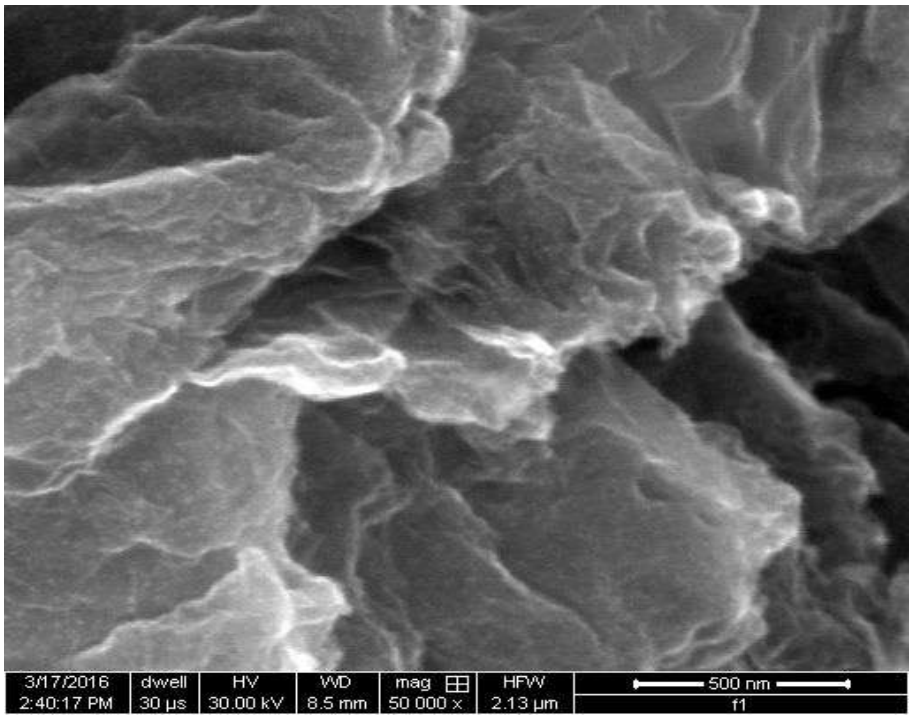

Figure 3.4b SEM image of rGO/ZrO_2 at low magnification

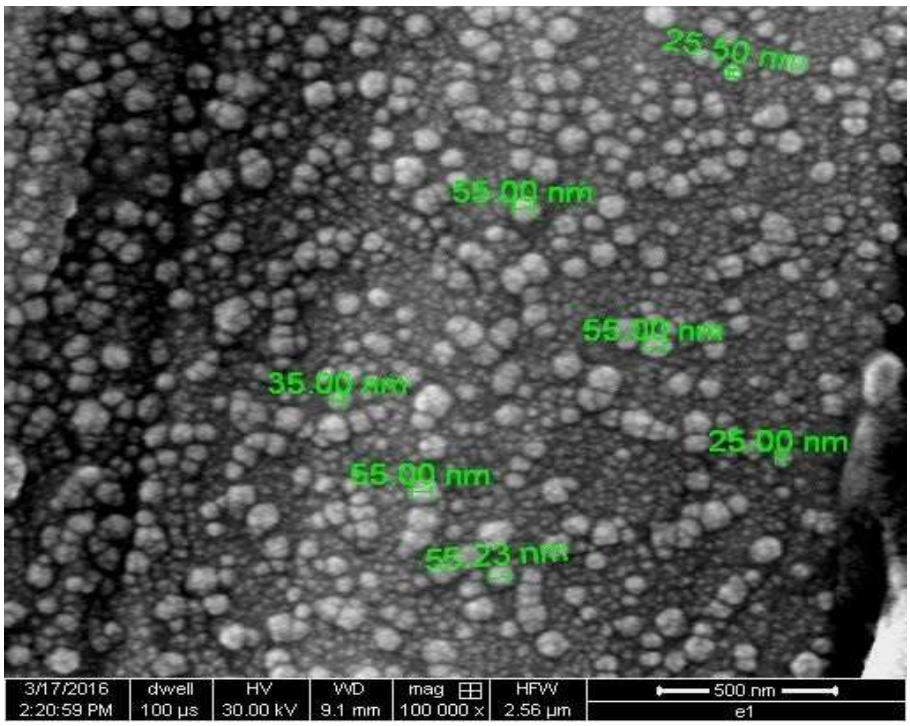

Figure 3. 4. (c) SEM image of rGO/ZrO_2 at high magnification

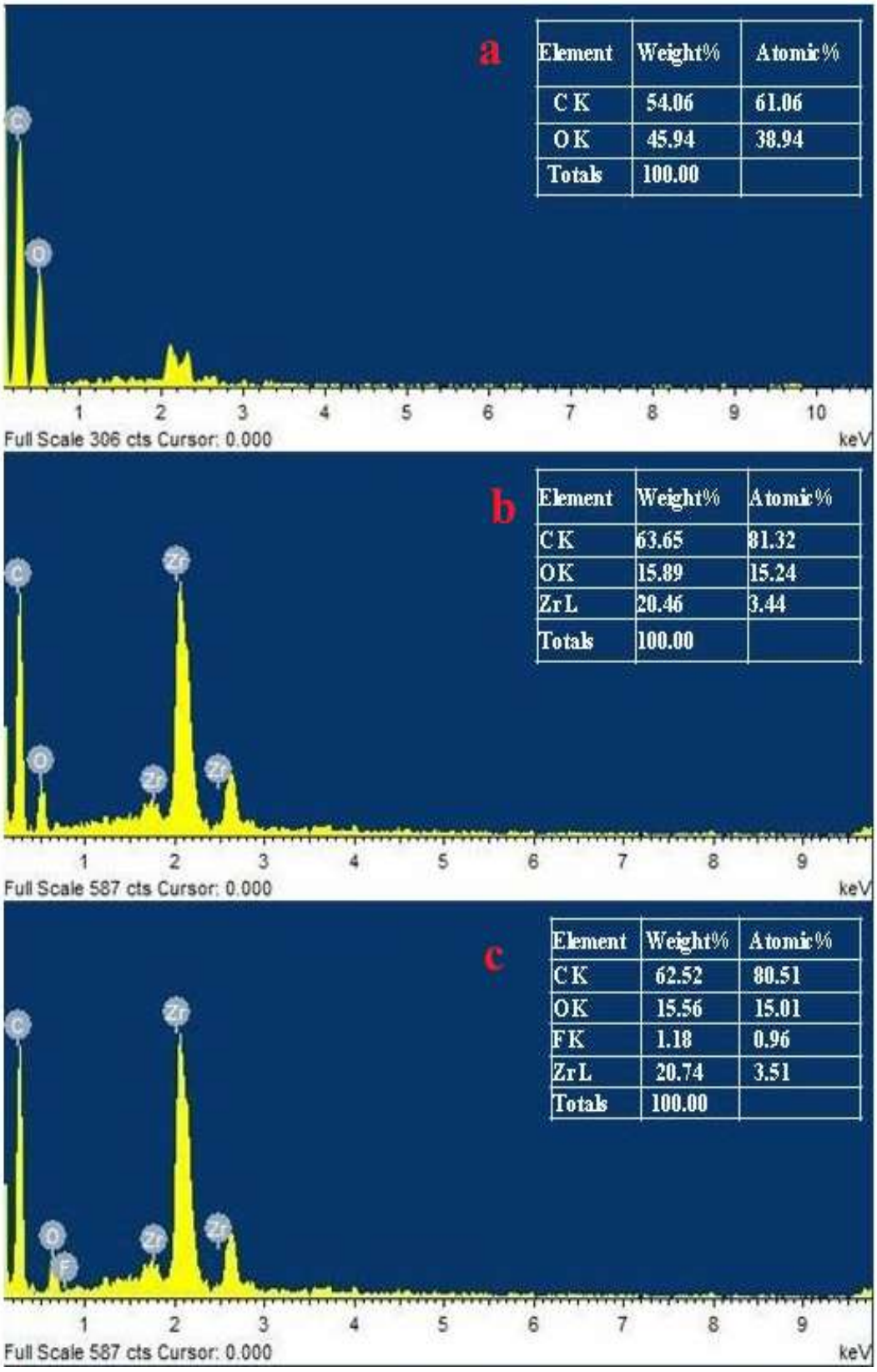

Figure 3.5 EDX spectrum (d) GO (e) rGO/ZrO_2 (f) rGO/ZrO_2 after fluoride removal

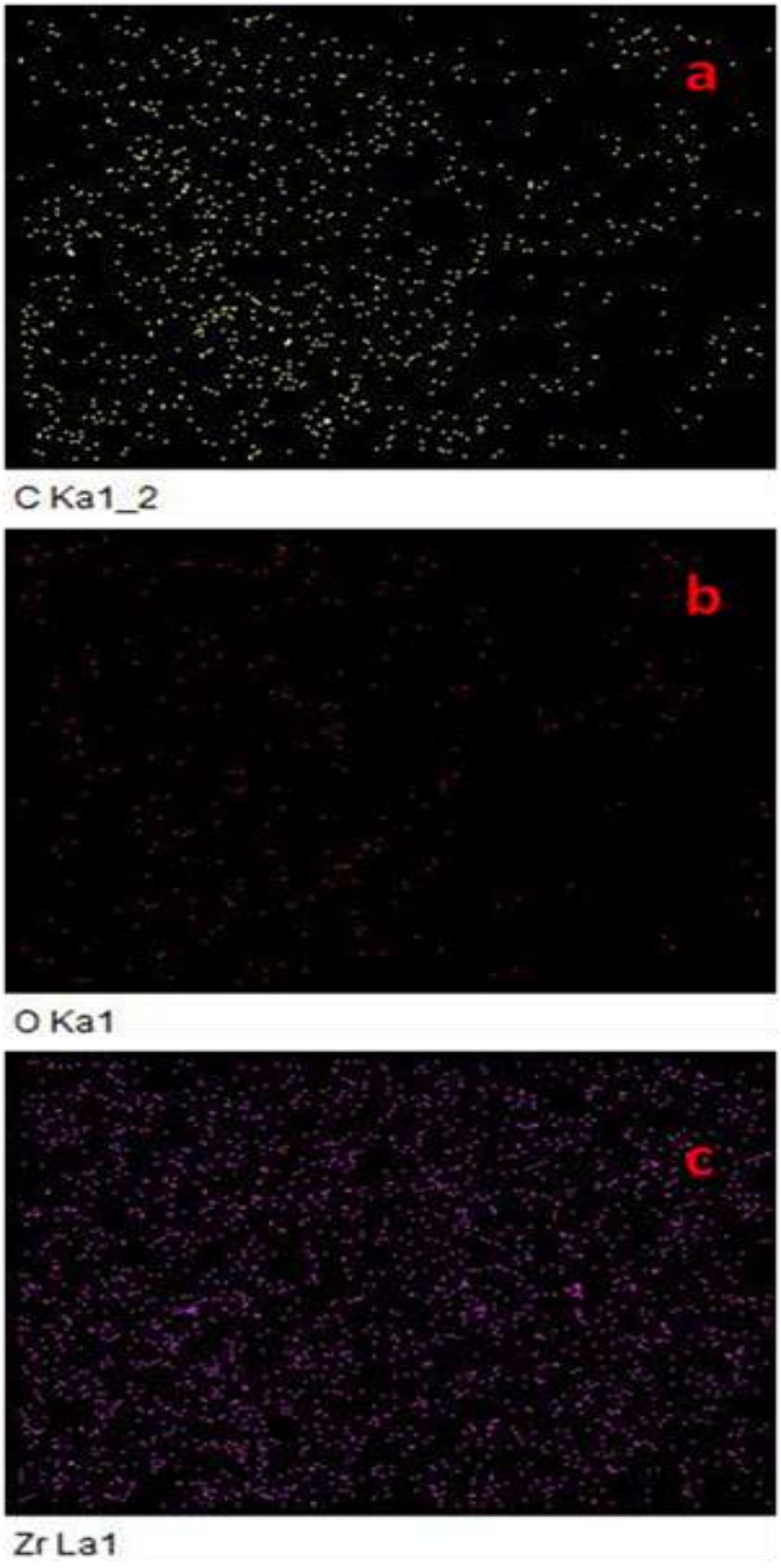

Figure 3.6 Elemental mapping of C, O and Zr

3.3.5 Raman analysis

Raman spectra were recorded with a Horiba JobinYvon, HR-800 Raman spectrometer using Ar ion laser (λ = 514 nm). The results of raman analysis **(**Figure 3.7) showed the characteristic pattern of the GO having two feature band at 1362 and 1599 cm^{-1} attributed to the D and G band respectively [Sreeprasad *et al.* (2011)]. It was also observed that after nanocomposite formation G band had experienced blue shift i.e. band was shifted to the lower frequency whereas, D band found to be unaltered which indicated toward the successful nanocomposite formation [Guo *et al.* (2015)].

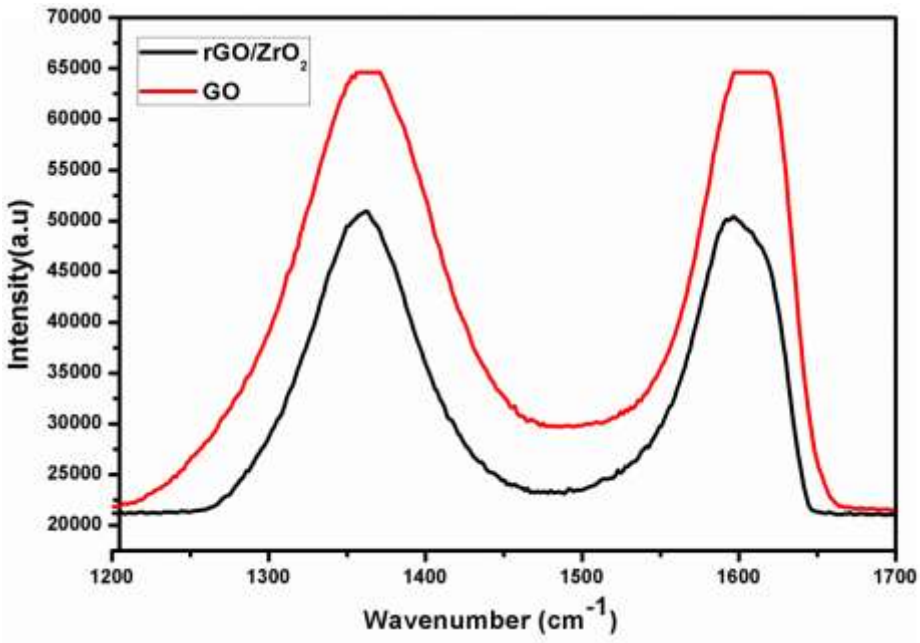

Figure 3.7 Raman analysis of GO and rGO/ZrO_2

3.3.6 Surface area measurement (BET)

Figure 3.8 represents the nitrogen adsorption-desorption curve of the prepared rGO/ZrO_2 nanocomposite. The specific surface area of the prepared nanoadsorbent was measured by Brunauer-Emmett-Teller (BET) method which was observed to be 632.67 m^2/g.

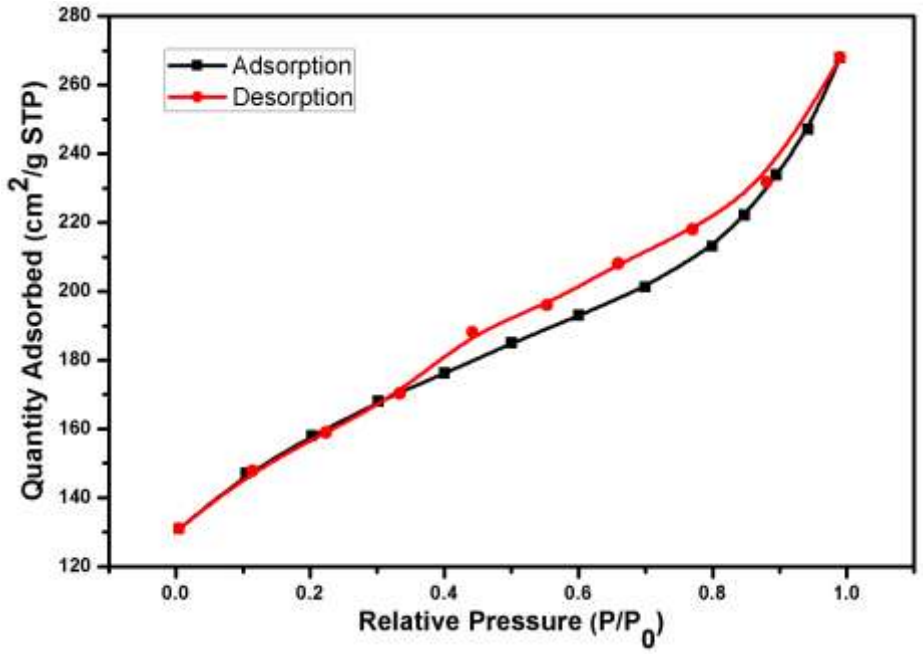

Figure 3.8 N_2 adsorption desorption isotherm of rGO/ZrO_2

3.3.7 Determination of pHzpc

The zero point charge pH of the nanocomposite was determined by solid addition method which is given in chapter 2 in detail. The graph of pH_i Vs. pH_f is shown in Figure 3.9. The pHzpc was found to be at pH 7.3 at which adsorbent surface acquires the neutral charge.

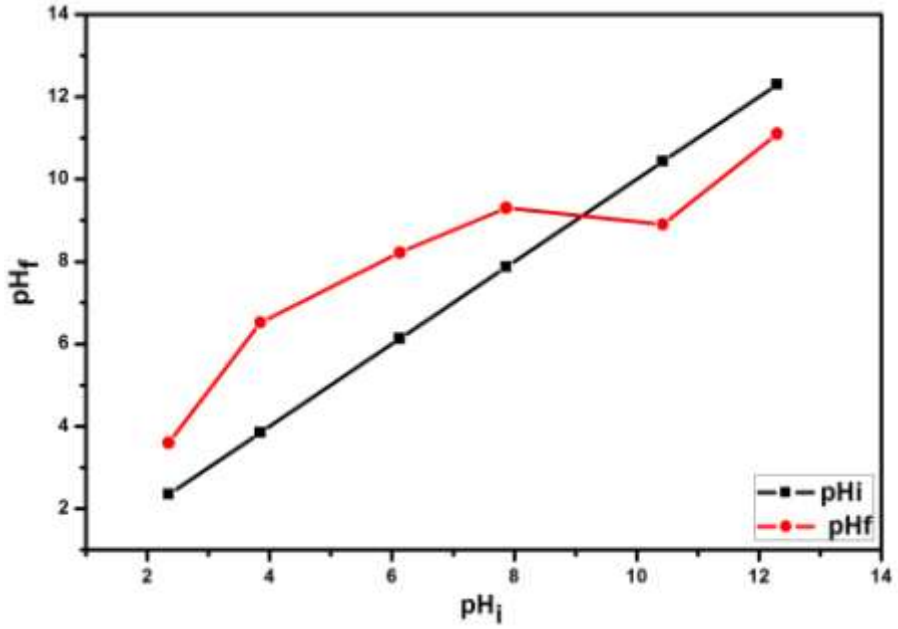

Figure 3.9 pHzpc curve of the rGO/ZrO_2

3.4 Batch adsorption studies

3.4.1 Effect of pH and mechanism of fluoride adsorption

The effect pH on fluoride adsorption was investigated in the pH range of 2 to 10 and keeping other parameters constant i.e. dose at 0.5g/L, temperature at 30°C, and initial fluoride concentration at 25 mg/L. Figure 3.10 shows the schematic representation of the effect of pH on adsorption capacity. The results indicated that rGO/ZrO_2 nanocomposite showed the maximum adsorption capacity at pH 7 i.e. neutral pH. The pHzpc of this adsorbent was found to be 7.3 which showed that the surface of the adsorbent bears negative charges if the pH>pHzpc while the adsorbent become positively charged when pH< pHzpc. Therefore, it was concluded that the pH below 7.3 was found to be suitable for fluoride adsorption for this adsorption system.

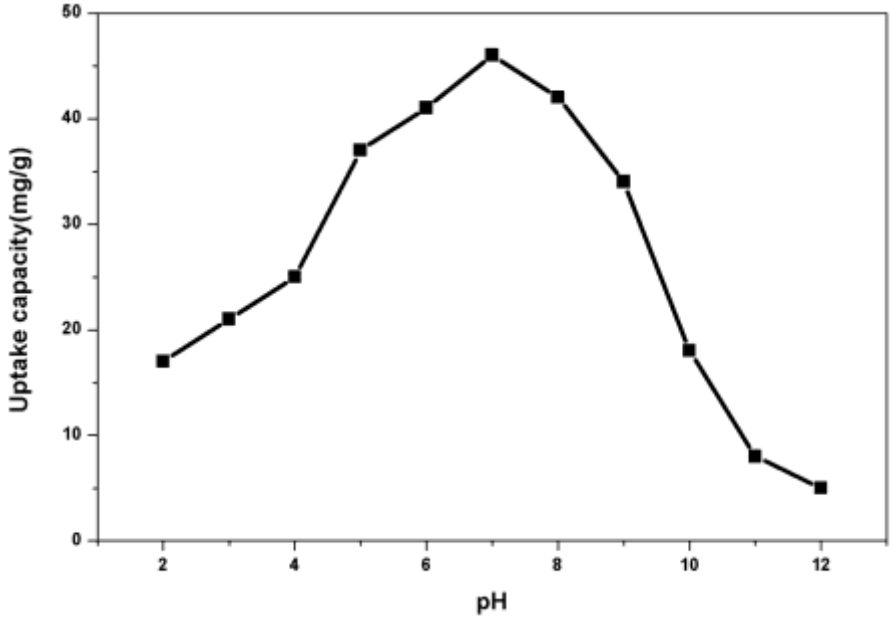

Figure 3.10 Effect of pH on uptake capacity

At low pH value, the reduction in uptake capacity was observed because fluoride gets protonated, and hydrofluoric acid was formed [Li *et al.* (2013)]. Furthermore, the uptake capacity falls substantially at pH>7 because at high pH value adsorbent become negatively charged which electrostatically repels the negatively charged fluoride. In addition to it, the OH^- concentration also increases at high pH values which compete with the fluoride for the binding sites of the adsorbent.

3.4.1.1 Mechanism of the fluoride adsorption

Adsorption of fluoride on the rGO/ZrO_2 involves the hard acid-base interaction in between Zr^{4+} and F^-. According to the HSAB principle, Zr^{4+} (classified as hard acid) and F^- (considered as hard base) interact very strongly because they show specific affinity for each other [Pearson **(**1963)]. In the solution, the ZrO_2 species exist as the

hydroxide form with which fluoride get interacts. In addition to electrostatic interaction, fluoride gets adsorbed by three following interaction.

Mechanism of adsorption [Chang *et al*. (2011)]

1. By electrostatic interaction

At low pH value protonation of the surface occur

$$\equiv Zr{-}OH + H^+ \rightarrow \equiv Zr{-}OH_2^+ \ (pH<pHzpc) \qquad (3.1)$$

At high pH values deprotonation of the surface occur

$$\equiv Zr{-}OH + OH^- \rightarrow \equiv Zr{-}O^- + H_2O \ (pH>pHzpc) \qquad (3.2)$$

2. By OH^- exchange or surface complexation.

$$\equiv Zr{-}OH + F^- \rightarrow \equiv Zr{-}F + OH^- \qquad (3.3)$$

$$\equiv Zr{-}OH_2^+ + F^- \rightarrow \equiv Zr{-}OH_2^+ \ F^- \qquad (3.4)$$

3. By hydrogen bonding

$$O\text{-}H + F^- \rightarrow O\text{-}H\cdots F^- \qquad (3.5)$$

Thus, it can be concluded that ligand exchange (complex formation), hydrogen bonding along with electrostatic interaction were the factors which are accountable for fluoride adsorption.

The adsorption of fluoride by OH^- exchange can be further explained by the probable surface reactions between ZrO_2 and F^- as represented from equation Eqs. 3.6 to 3.13. It is clearly represented by the equations that one molecule of ZrO_2 could bind with five F^- ion which is responsible for increasing uptake capacity of rGO/ZrO_2 nanocomposite [Teutli-Sequeira *et al*. (2015)]. Since, the pHzpc rGO/ZrO_2 is found to

be 7.3 therefore, its protonation and deprotonation occurs below and above the pH 7.3 respectively which are represented in eq. 3.6 and 3.7. In the aqueous solution, the ZrO_2 exists as seven coordinated polyhedral species [Dou *et al.* (2012)]. The protonated hydroxyl groups of ZrO_2 facilitate the attachment of F^- ion to which is represented in Eq. 3.8.

In Eq. 3 the attack of F^- at ZrO_2 took place via an associative mechanism by expanding the coordination number from seven to eight which was followed by the loss of water to give the seven-coordinated monofluorinated species. The same process also occurred in equations from 3.9 to 3.13. For addition of each F^- ion and to form di-, tri-, tetra- and pentafluoro zirconium species, three consecutive steps i.e. hydroxyl protonation, fluoride ion attack and loss of water molecule take place. After the formation of pentafluoro zirconium species, the protonation of a hydroxyl group or Zr–O–Zr bridging oxygen group becomes difficult due to reason that on the attachment of F^-basicity of these oxygen decreased.

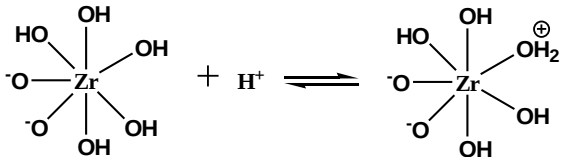

(3.6)

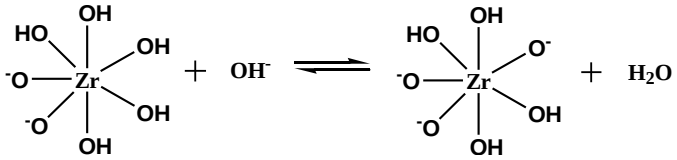

(3.7)

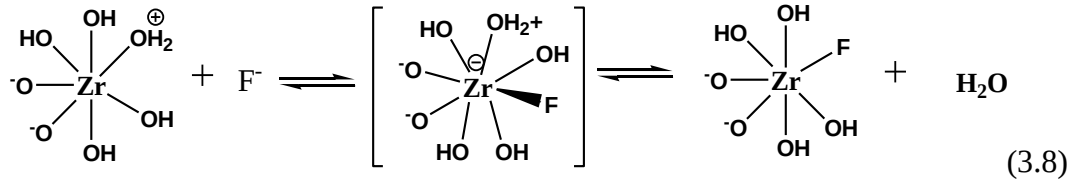

(3.8)

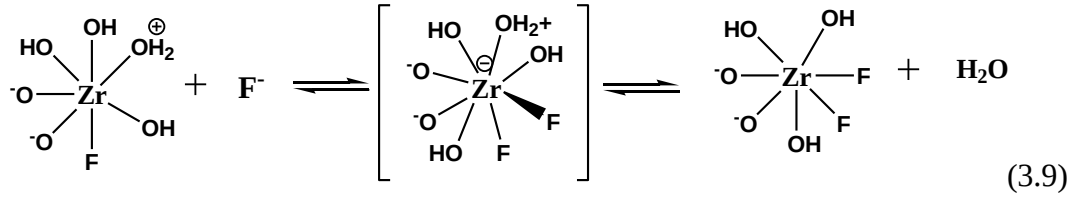

(3.9)

(3.10)

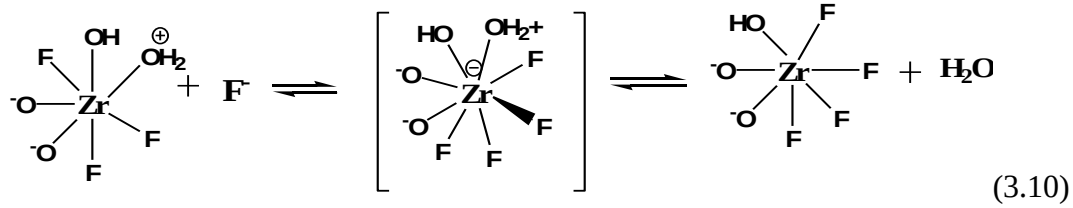

(3.10)

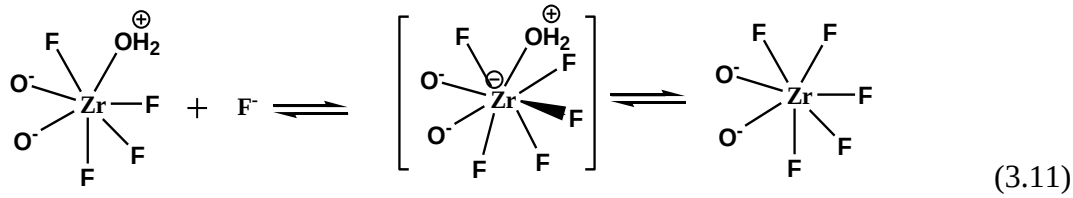

(3.11)

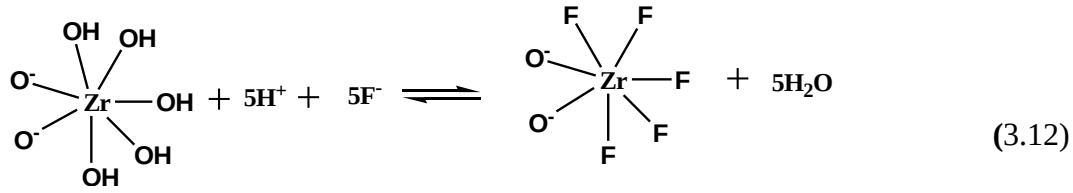

(3.12)

3.4.2 Effect of contact time and rGO/ZrO_2 dose on the uptake capacity

The effect of contact time on adsorption capacity was studied at three different doses (0.4, 0.5 and 0.6 g/L) in between the time period of 0-100 minutes. Figure 3.11 represented the pictorial presentation of variation of uptake capacity on contact time. Effect of contact time was evaluated at the constant initial fluoride concentration of 25

mg/L, temperature 30°C and pH 7. The result showed that the adsorption was initially very high which indicated, that the rate of adsorption was very rapid because the active binding sites of rGO/ZrO_2 were free and the concentration gradient of fluoride was also high. But as the time advanced, the rate of adsorption decreased due to the reduction in the number of free binding sites and the concentration gradient of fluoride. It was also observed that the equilibrium time did not depend on the rGO/ZrO_2 dose. Therefore, the equilibrium time was 50 min at all rGO/ZrO_2 doses. The uptake capacity increased slightly with the increase in dose from 0.4g/L to 0.5g/L whereas, on increasing the adsorbent dose from 0.5 g/L to 0.6 g/L it decreased remarkably.

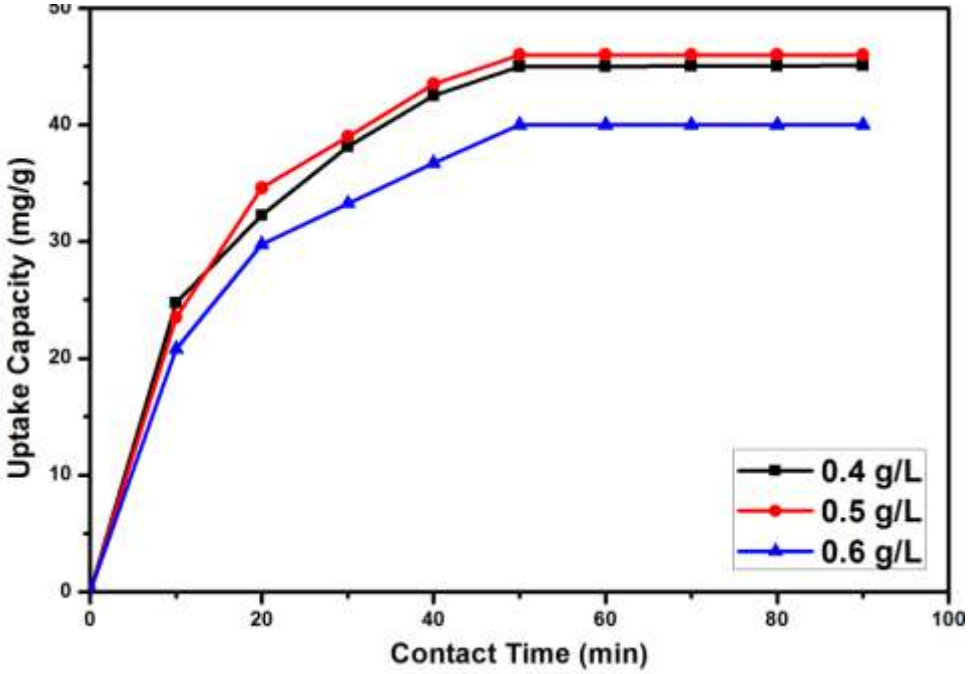

Figure 3.11 Effect of contact time and dose on uptake capacity

The reduction in uptake capacity occurs at higher dose since the uptake capacity depends on the adsorbate-to-binding site's ratio which decreased on increasing the rGO/ZrO_2 dose 0.5 to 0.6 g/L. That's why at higher rGO/ZrO_2 doses the available fluoride became insufficient to cover all the binding sites of the adsorbent.

3.4.3 Effect of initial concentration and temperature on the uptake capacity

The effect of fluoride concentration on the adsorption performance of prepared nanoadsorbent was analysed in the concentration range of 5 to 50 mg/L. Experiments were performed at constant pH (7), rGO/ZrO_2 dose (0.5 g/L) at different temperatures (20°C, 30°C, and 40°C) and the results are displayed in the Figure 3.12. The above graph revealed that the uptake capacity was increased with an increase in fluoride concentration up to 25 mg/L. After that, uptake becomes stagnant i.e. no further increase in adsorption capacity was observed. Thus, the 25mg/L of fluoride concentration was considered as optimum concentration which is enough to cover approximately all the active binding sites of the 0.5 g/L of rGO/ZrO_2 dose. It was also found that the uptake capacity was also dependent on reaction temperature. As the temperature rises from 20-30°C uptake capacity increased from 38 to 46 mg/g while it declines from 38 to 46 mg/g with further increase in temperature from 30-40°C. Therefore, 30°C temperature was found to be optimum for fluoride adsorption at which maximum adsorption occurred. Since high temperature (above 30°C) become the limiting factor for the adsorption as the randomness increased with temperature which acts as a retardation factor for the adsorption [Singh *et al.* (2016)].

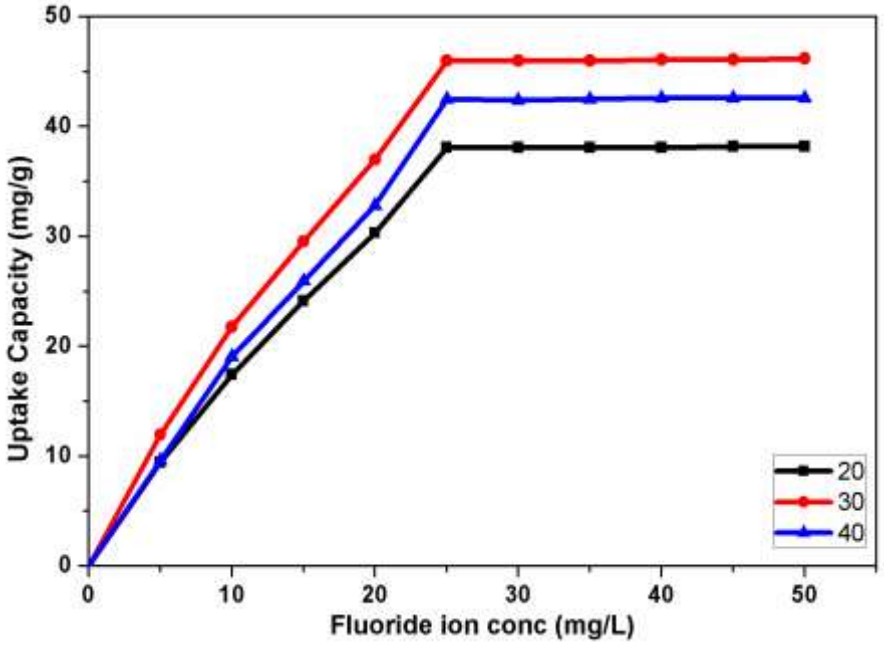

Figure 3.12 Effect of fluoride concentration and temperature on uptake capacity

3.5 Kinetic studies

The experimental data were subjected to various kinetic model to determine the rate controlling step and different important kinetic parameters. For this investigation, the kinetic experiments were carried out at three different doses i.e. 0.4, 0.5, and 0.6 g/L.

3.5.1 Pseudo-first-order and pseudo-second-order kinetic models

The various important kinetic parameter related with Pseudo-first-order was calculated by the plot of log (qe-qt) *vs.* t (min) (Figure 3.13**)** at all given doses and is summarized in Table 3.1 Whereas, the kinetic parameters and R^2 values corresponding to the pseudo-second-order model are presented in Table 3.1 which was determined

from the respective plots of t/q_t versus t (min) at different doses (Figure 3.14). The results showed that the value of regression coefficient (R^2) is appreciably high for pseudo-second-order model than that of pseudo-first-order kinetic model which indicated that this adsorption system is better explained by pseudo-second-order kinetic model. Thus the rate of adsorption found to be proportion to the square of free binding sites $(qe-qt)^2$ on the adsorbent. It was also found that the rate constant was observed to be increased with increase in dose of the rGO/ZrO_2 which was considered as proof for the suitability of this kinetic model for the adsorption of fluoride on rGO/ZrO_2 nanocomposite.

3.5.2 Mass transfer studies

The coefficient of mass transfer was calculated from the Mckay et al. was found to be 3.7×10^{-3}, 6.7×10^{-3}, 5.2×10^{-3} which was calculated from the plots of $\ln((Ct/Ci)-1/(1+mK))$ vs. t (min) and shown in Figure 3.15 at three different doses 0.4, 0.5, 0.6 g/L. Results displayed that the values of β_t are quite high which suggested that the mass transfer from boundary film to surface of the adsorbent has occurred very rapidly. Thus it was concluded that rGO/ZrO_2 was suitable for fluoride removal and also this step does not involve in rate controlling process.

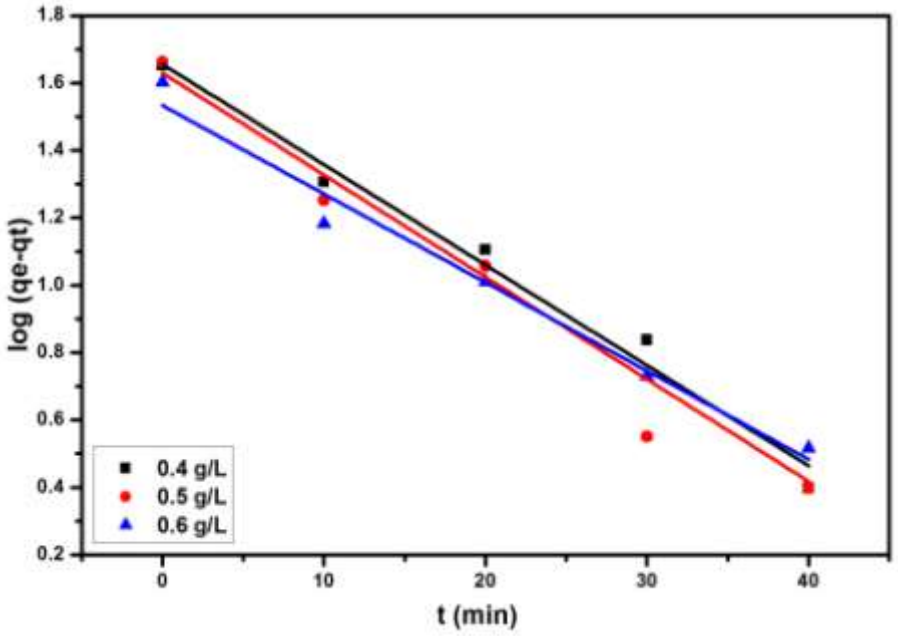

Figure 3.13 Pseudo-First-order kinetic model

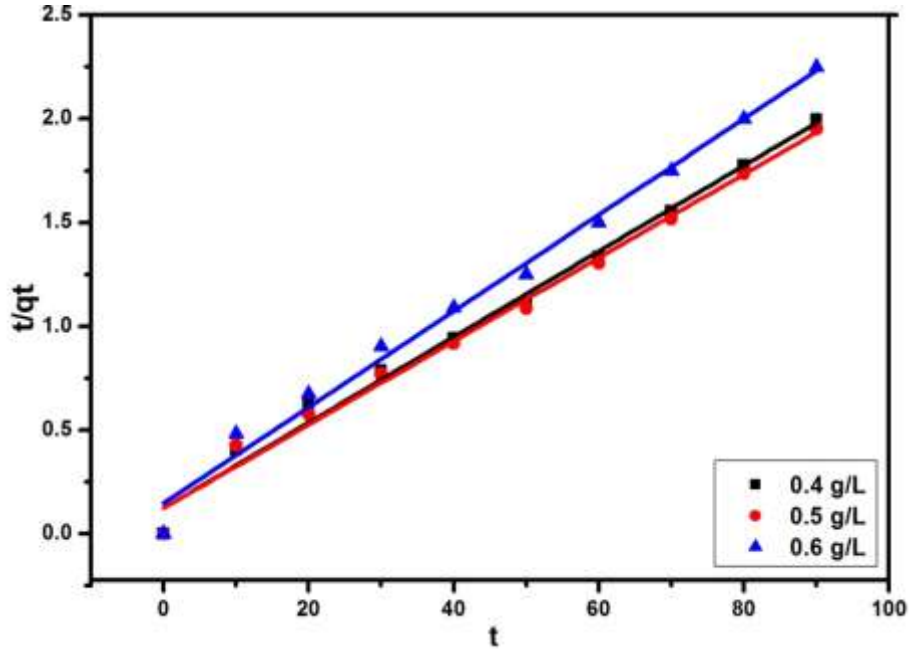

Figure 3.14 Pseudo-Second-order kinetic model

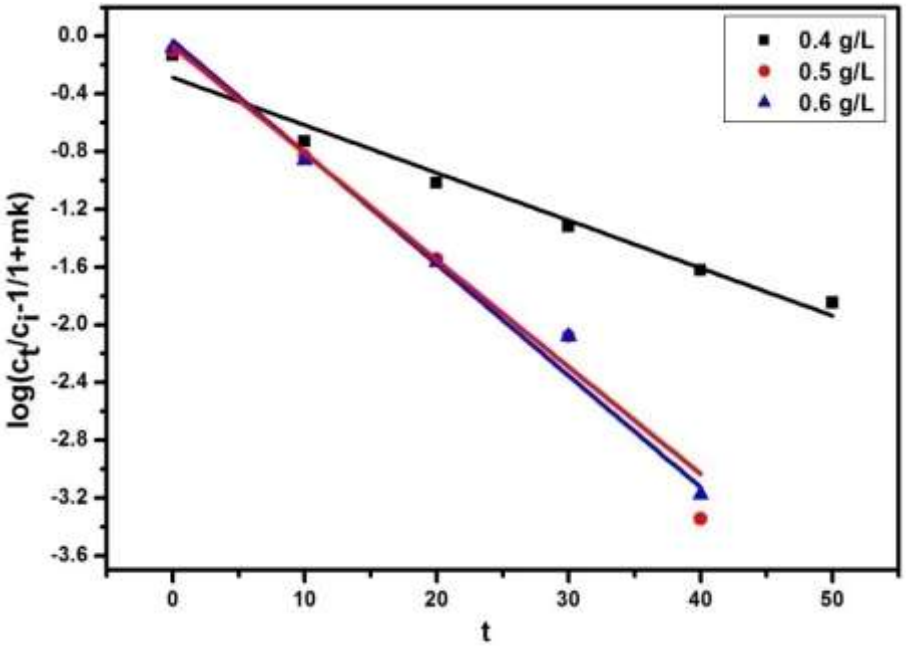

Figure 3.15 Mass transfer plot at different rGO/ZrO_2 dose

3.5.3 Intra particles diffusion model

Figure 3.16 represents the plot of qt *vs.* $t^{0.5}$ (min) corresponding to the Weber-Morris model of intraparticle diffusion. It is well-reported in the literature that "if the plot of intraparticle diffusion is linear and passed through origin then it will be considered as rate determining step [Viswanathan and Meenakshi (2009)]. In this case, the plots are significantly linear although they do not pass through origin which suggested that the fluoride adsorption proceeds by means of a complex mechanism in which mass transfer as well as intraparticle diffusion both actively involved.

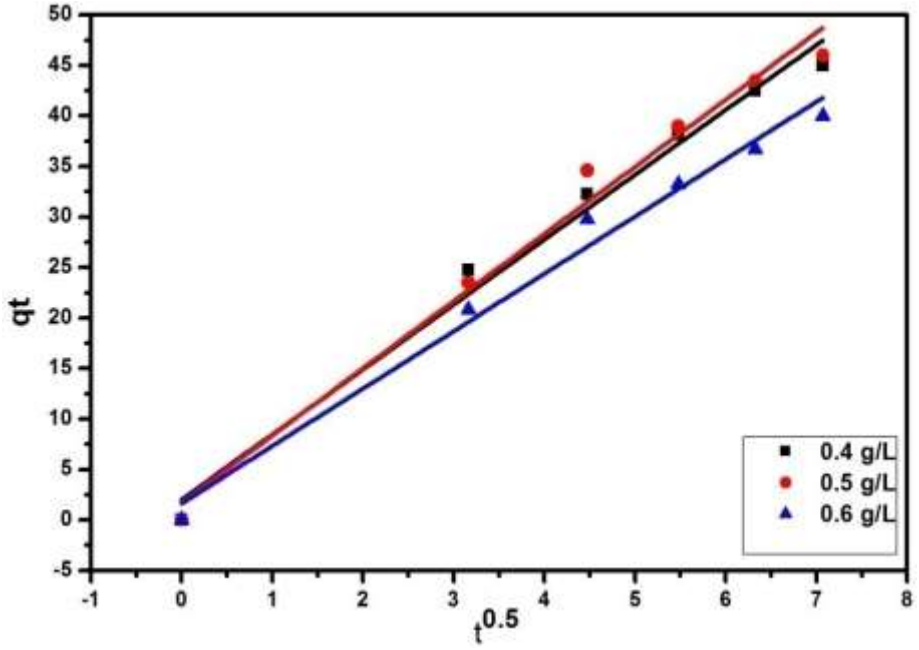

Figure 3.16 Intraparticle diffusion plot at different rGO/ZrO_2 dose

3.5.4 Richenberg Model

The plot of B_t vs. t (min) represents the corresponding Richenberg Model kinetics which is used to examine the possibility of intraparticle diffusion as the rate controlling step of this adsorption system. Results (Figure 3.17) showed that the plots are significantly linear and having high R^2 values. However, these plots did not pass through the origin. Therefore, it was concluded that rate of the reaction did not depend only on intraparticle diffusion which supports the finding of the Weber-Morris model [Hasan *et al.* (2008)].

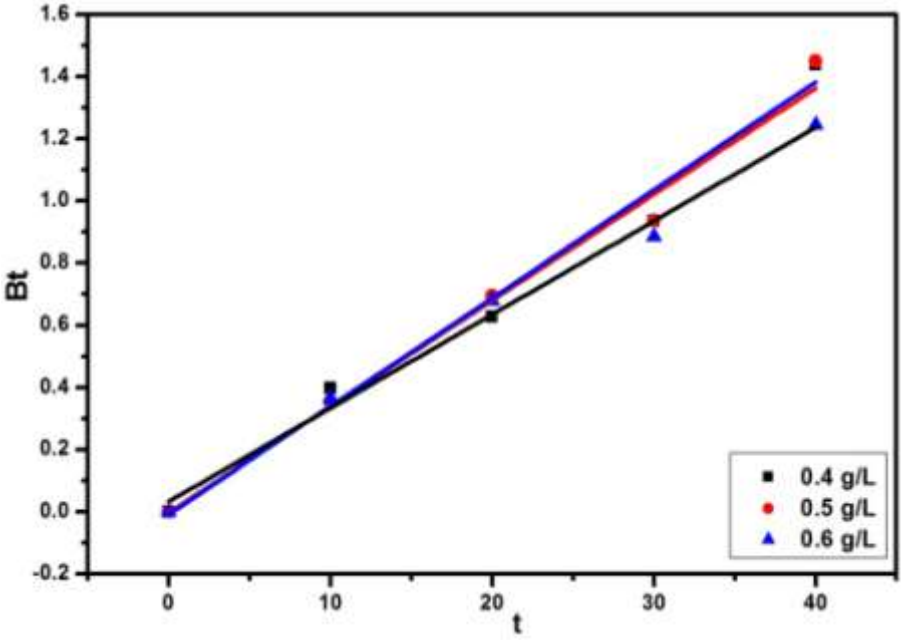

Figure 3.17 Richenberg plot at different rGO/ZrO_2 dose

Table 3.1 Kinetic parameters for the adsorption of fluoride at different rGO/ZrO_2 doses

Model Parameters	Fluoride concentration		
	0.4g/L	**0.5g/L**	**0.6g/L**
Pseudo-first-order			
K_1 (min^{-1})	0.0741	0.074	0.069
qe (exp.)(mg/g)	45	46	40
qe (cal.) (mg/g)	48.8	50.03	41.98
R^2	0.981	0.985	0.972
Pseudo-second-order			
K_2'	0.0024	0.0024	0.0034
qe (mg/g)	48.5	49.75	43
R^2	0.990	0.992	0.997
Mass Transfer			
$\beta_t \times 10^{-3}$ (cm^2/sec)	2.5	4.6	3.6
R^2	0.972	0.984	0.980
Interparticles Diffusion			
K_{id}(mg/g.$min.^{0.5}$)	6.42	6.64	5.68
C	2.03	1.73	1.65
R^2	0.986	0.984	0.989

3.6 Isotherm studies

The experimental equilibrium data for the fluoride adsorption onto rGO/ZrO2 were applied to the most widely used models such as Freundlich, Langmuir and D-R isotherm model. These models were utilized to predict the mathematical relationship in between amount of adsorbate adsorbed per gram of adsorbent (q_e (mg/g)) to the equilibrium solution concentration (C_e(mg/L)) at a constant temperature. The isotherm experiments were conducted by varying initial fluoride concentration from 5 to 50 mg/L at three different temperature i.e. 20, 30 and 40°C by keeping other parameters constant adsorbent dose (0.5 g/L) and pH (7) constant.

3.6.1 Freundlich Isotherm

Figure 3.18 displayed the plot of log ce versus log qe corresponding to the Freundlich isotherm model. The different isotherm constant (n and k_f) and R^2 values obtained from the plots at three different temperatures are given in Table 3.2. The value of n lies in between 1 to 10 which supports the favorable adsorption of fluoride on the rGO/ZrO_2 [Ranjan *et al.* (2009)]. In addition to it, the value of k_f (sorption capacity) was increased with the rise in temperature which indicated the endothermic nature of this adsorption system.

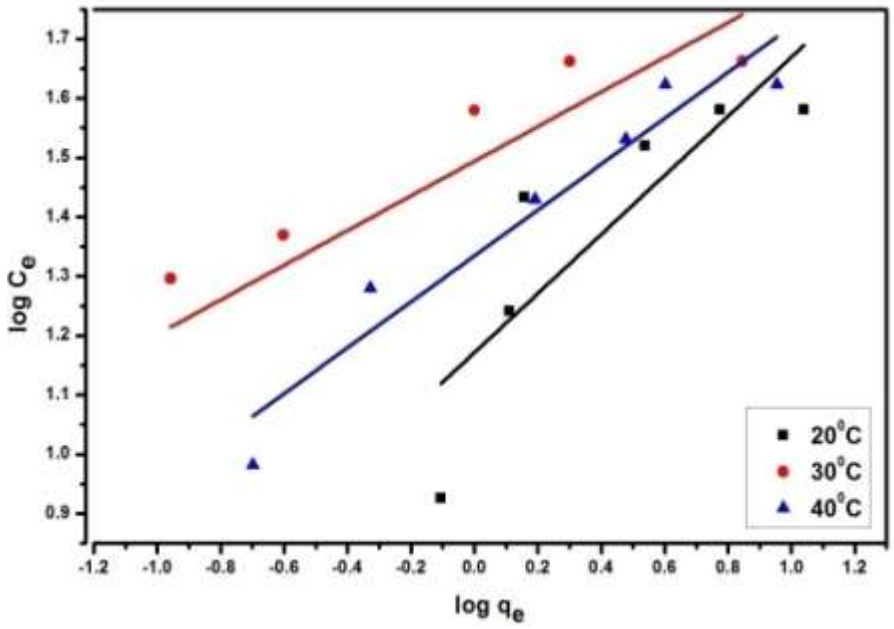

Figure 3.18 Freundlich isotherm plots at different temperatures

3.6.2 Langmuir Isotherm

A graph of C_e/q_e versus C_e at variable temperature is shown in Figure 3.19 from which Langmuir parameters (Q^0 and b) were calculated which are given in Table 3.2. The plots were found to be significantly linear, and the high values of R^2 advocated for the applicability of Langmuir isotherm for this adsorption system. Thus it was also concluded that the adsorption was monolayered and active sites are homogenously energized. The maximum uptake capacity (Q°) at pH 7 and temperature 30°C was found to be 46.9 mg/g and its value increased with increase in temperature. Thus, the endothermic nature of adsorption system also supported by this isotherm study. Another important dimensionless parameter, R_L which is known as separation factor was also calculated with the help of following equation:

$$R_L = \frac{1}{1+bC_0} \tag{3.13}$$

where b and C_0 represent the Langmuir constant and initial fluoride concentration respectively. The factor R_L provides an idea about the adsorption process whether it is feasible or not [Bharali and Bhattacharyya (2015)]. If the value of R_L lies in the range of $0 < R_L < 1$ the adsorption will be favorable and in this case RL value was calculated to be 0.0399 for the fluoride adsorption by rGO/ZrO_2. Thus, the value of R_L also indicated that the fluoride adsorption onto rGO/ZrO_2 nanocomposite was favorable.

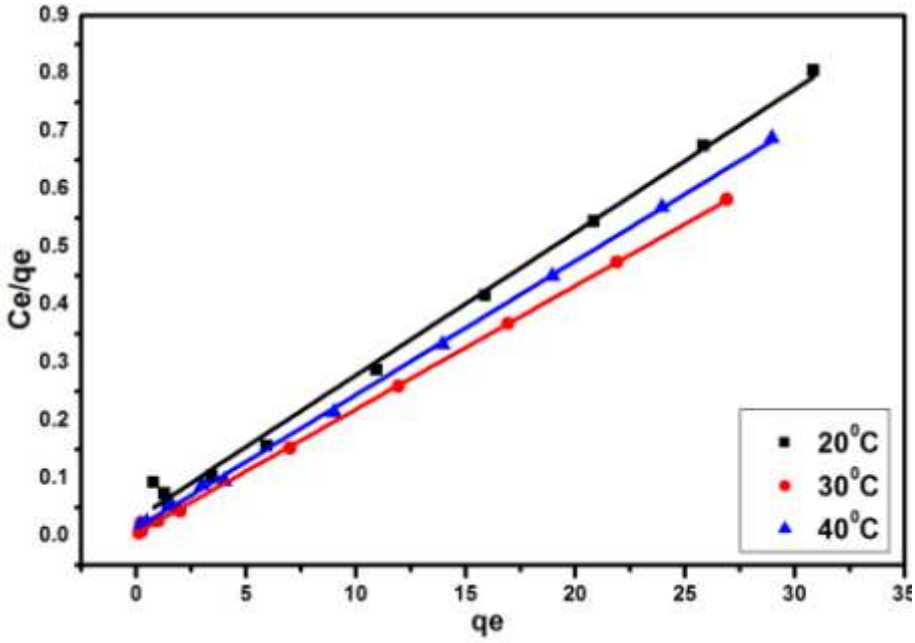

Figure 3.19 Langmuir isotherm plots at different temperatures

3.6.3 D-R Isotherm

Figure 3.20 represents the plot of ln qe vs. F^2 from which important parameter of D-R isotherm was calculated and are given in Table 3.2. It was observed that the plots are considerably linear at all mention temperatures which was revealed by the high value of R^2. The values of E (kJ/mol) i.e. energy of adsorption was also determined at all temperatures and the values found to be in the range which is specified for the chemisorption behavior of adsorption process. Overall, it was concluded that the D-R isotherm model fits well to the equilibrium adsorption data and fluoride adsorbs on the rGO/ZrO_2 by chemical interactions also.

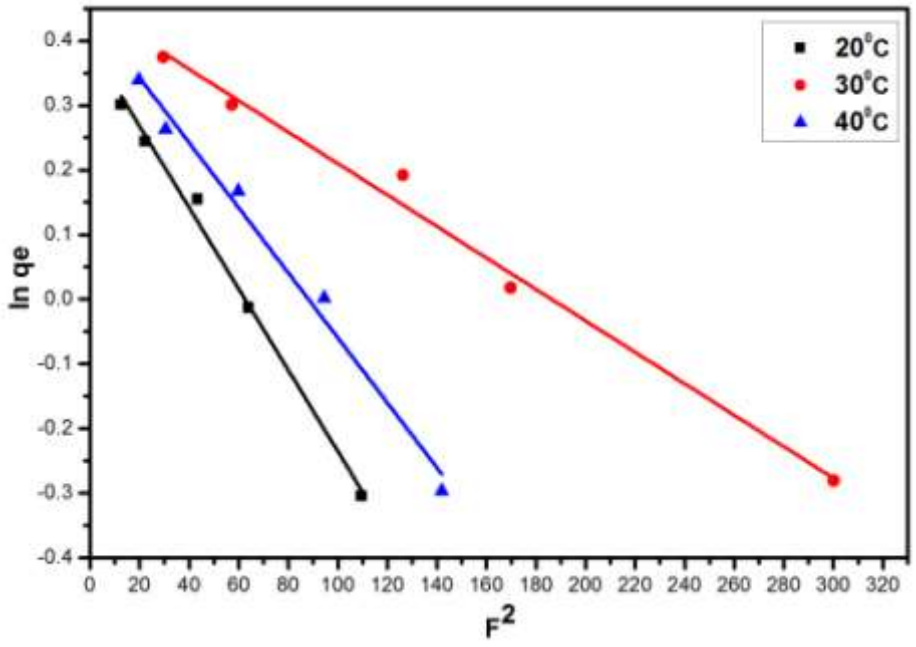

Figure 3.20 D-R isotherm plots at different temperatures

Table 3.2 Parameters of Langmuir, Freundlich and D-R isotherm for the adsorption of fluoride at different temperature

Temperature	Freundlich Parameters			Langmuir Parameters			D-R Parameters		
	k_f (mg/g)	n	R^2	Q^0 (mg/g)	b (L/mg)	R^2	X_m (mmol/g)	E (KJ/mol)	R^2
20°C	16.59	3.33	0.60	40.49	0.0007	0.99	0.995	14.43	0.99
30°C	28.18	5.12	0.65	47	0.0001	0.99	0.995	9.12	0.99
40°C	20.89	3.80	0.893	43.3	0.0003	0.99	0.995	10	0.99

3.7 Thermodynamics Studies

Van't Hoff graph was plotted n between ln k_c versus 1000/T (Figure 3.21) from which important thermodynamic parameters (ΔG^0, ΔH^0, ΔS^0) were calculated from slopes and intercepts. The values of ΔG^0, ΔH^0, ΔS^0 have listed in Table 3.3. Results depicted that this adsorption process was spontaneous at all studies temperature which was showed by negative value of ΔG^0. In addition to it, the spontaneity was increased with increase in temperature which indicated the endothermic nature of current adsorption system. The value of ΔH^0 (kJ/mol) found to be positive which again supported the endothermic nature of the adsorption. Furthermore, the positive value of ΔS^0 indicated that the randomness was increased in this adsorption system, and the reason behind this process is that the desorption also takes place along with the adsorption at the solid-liquid interface which increases the disorderliness of the system [Argun *et al.* (2007), Hefne *et al.* (2008)].

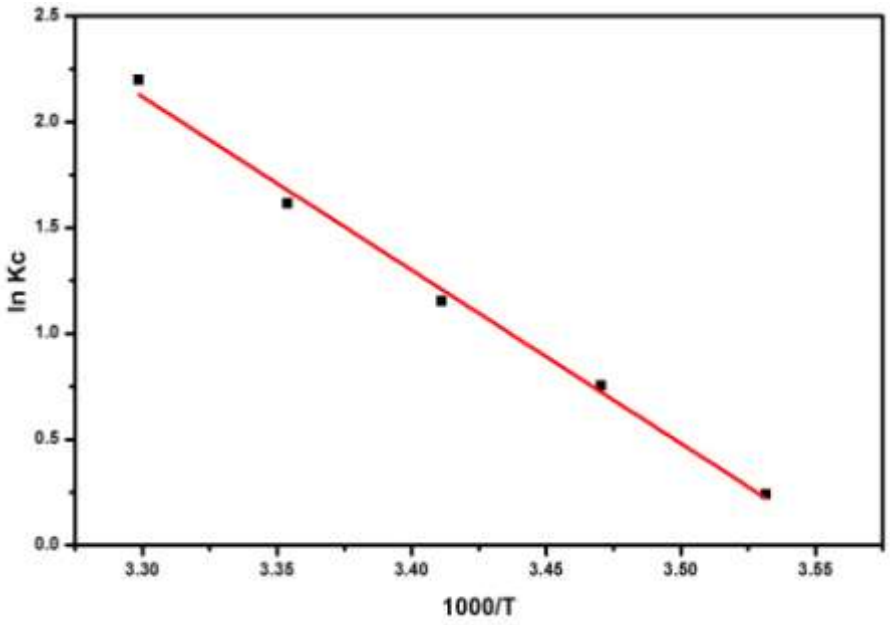

Figure 3.21 Van't Hoff plot for the adsorption of fluoride on the rGO/ZrO_2

Table 3.3 Thermodynamic parameters for the adsorption of fluoride on the rGO/ZrO_2

Temperature	ΔG(kJ/mol)	ΔH(kJ/mol)	ΔS(kJ/mol/ K)
20°C	-2.80464	0.07698	0.272008
25°C	-3.99468		
30°C	-5.52854		

3.8 CONCLUSION

In this work, the efficacy of the rGO/ZrO_2 nanocomposite was tested for the adsorptive remediation of fluoride from water. The nanocomposite (rGO/ZrO_2) was prepared by hydrothermal method which was observed to be highly efficient and showed high uptake capacity of 46 mg/g for fluoride. The rGO/ZrO_2 showed maximum adsorption capacity of 46 mg/g at neutral pH and 30°C temperature. The adsorption equilibrium established in very short period of time i.e. in 50 min. The kinetic studies revealed that this adsorption system follows pseudo-second-order kinetics which also supported the fast adsorption of fluoride onto rGO/ZrO_2 nanoadsorbent. The kinetic study also indicated that intraparticle diffusion along with external mass transfer takes part in rate determining step. It was also found that Langmuir isotherm fitted well to the equilibrium data; thus, it was confirmed that the adsorption was monolayer. Thermodynamic studies advocated that this adsorption system was spontaneous while the ΔH^0 value observed to be positive which indicated that adsorption process was endothermic in nature. The above discussion provides fundamental information which are useful to design the continuous column studies for the removal of fluoride by rGO/ZrO_2.